Advanced Ceramics Progress: Vol. 9, No. 4, (Autumn 2023) 7-14

Materials and Energy Research Center
MERC

Contents lists available at ACERP

Advanced Ceramics Progress

Journal Homepage: www.acerp.ir

Original Research Article

Investigation on the Band Gap of Centered Square Phononic Crystals

Bentolhoda Amanat [a]*, Mohammad Reza Kazerani Vahdani [b]

[a] *Assistant Professor, Department of Physics, Payame Noor University, Tehran, Iran.*
[b] *Associate Professor, Faculty of Naval Aviation, Malek Ashtar University of Technology, Iran.*

* Corresponding Author Email: amanat@pnu.ac.ir (Bentolhoda Amanat)

URL: https://www.acerp.ir/article_181825.html

ARTICLE INFO

Article History:

Received: 17 September 2023
Revised: 22 October 2023
Accepted: 25 October 2023

Keywords:

Phononic Crystal,
Band Gap,
Piezocomposite,
Filling Fraction

ABSTRACT

The periodic structure of 1-3 piezocomposite phononic crystal minimize the effect of the coupling of parasitic modes on the deliberately excited plane modes and prevent the propagation of unwanted Lamb waves. In this article, the band structures of the centered square phononic crystals of PZT-5H rods in polyethylene terephthalate matrix was studied using the numerical method of finite elements. In particular, the phoninic band gaps of the system was investigated as the functions of the volume of the PZT element at the center of the unit cell of the considered crystal under the constant filling fraction of PZT rods. According to the results, the band structure of the system contains three gaps whose widths vary by the volume. These gaps are extended in the (normalized) frequency range of 1100-2530 m/s. Further observations particularly show that in case the all PZT rods of the system are of the same size, the maximum achievable band gap of the system will be obtained.

https://doi.org/10.30501/acp.2023.416606.1131

1. INTRODUCTION

Today, piezocomposite materials are used in many engineering applications and smart structures. The concept of piezocomposite materials was first introduced in 1978 by Newnham et al., which garnered significant attention and recognition (H. Wang et al., 2022). In piezocomposite structure, a piezoelectric material with high piezoelectric properties, such as PZT and PMN-PT, typically serves as an active phase while a polymer material, such as epoxy resin, polyethylene, etc., acts as an inactive phase (Amanat, 2022) (Lv et al., 2022). Based on the connection concept proposed by Newnham, these materials are classified into 10 types of piezocomposites (Tize Mha et al., 2021). One of the most renowned and widely used materials is 1-3 piezocomposite.

The superior properties of piezocomposites, namely low acoustic impedances (ranging from 5 MRayl to 27 MRayl), high coupling coefficients (usually in the range of 0.61 to 0.75), high bandwidth and lower Q_m, have made these materials widely applied in high frequency ultrasound transducers, medical imaging, and sonar systems (Behera, 2022) (Zhou et al., 2021). The periodic structure of piezocomposites causes the formation of specific stop bands or band gaps in the frequency spectrum of these structures. The presence of these band gaps drawn the attention of numerous scientists in recent years to the propagation of elastic waves in heterogeneous media (Y.-Z. Wang et al., 2009). In fact, the large band gaps in piezocomposites find applications in elastic and acoustic filters, transducer structures,

Please cite this article as: Amanat, B., Kazerani Vahdani, M. R., "Investigation on the Band Gap of Centered Square Phononic Crystals", ***Advanced Ceramics Progress***, Vol. 9, No. 4, (2023), 7-14. https://doi.org/10.30501/acp.2023.416606.1131

control of noise, and vibration shields (Vatanabe & Silva, 2011). For instance, by tuning the frequency of the thickness mode of piezocomposites within these band gaps, it is possible to minimize coupling with parasitic modes, such as lateral modes, and prevent the propagation of Lamb waves. Consequently, substantial research efforts have been devoted to broadening the band gap widths (Sigmund & Jensen, 2003) (Wu et al., 2009), a characteristic which strongly depends on the physical properties, size, and shape of constituent phases (Miranda & Dos Santos, 2022).

Hou et al. (Hou et al., 2004) investigated the elastic band gap structure of a two-dimensional acoustic crystal containing piezoelectric materials and analyzed the piezoelectric effects on the band gaps. Qian et al. (Z. Qian et al., 2004) studied the dispersion relations of horizontal shear wave propagation in a periodic layered piezoelectric structure for cases of wave propagation in normal and tangential directions to the interface. Silva et al. (Vatanabe et al., 2014) attempted to maximize the absolute elastic wave gap width in designed piezocomposite materials using topology optimization. Zheng Hua et al. (Z.-H. Qian et al., 2008) compared the band gaps in two-dimensional piezocomposite with 1-3 connection family of piezoceramic rods, which had circular and square cross-sections. Sigmund (Sigmund & Jensen, 2003) (Thompson & Sigmund, 2000) applied the topology optimization to design periodic materials and structures with acoustic band gaps to minimize the structural response along the boundaries or maximize the response at certain boundary points. Halkjer et al. (Halkjaer et al., 2005) maximized the acoustic band gap for infinite periodic beam structures modeled based on Timoshenko beam theory, considering alternating, thick and medium thickness plates, and finite thick plates. Jensen et al. (Halkjær et al., 2006) extended the bandgap size for shear waves in the Mindlein plane. Evgrafov et al. (Rupp et al., 2007) applied topology optimization to the design of 2D and 3D phononic (elastic) materials, focusing on the surface wave filters and waveguides. Other different aspects related to the propagation of sound waves in two- and three-dimensional piezoelectric periodic structures have been addressed in several research studies (Vashishth & Gupta, 2009) (Y.-Z. Wang et al., 2007) (Y.-S. Wang, 2008) (Vu Quoc et al., 2021).

Most of the past research projects were primarily based on three main axes: a) adjusting the piezoceramic filling fraction, leading to changes in the piezocomposite parameters such as coupling coefficient, characteristic impedance, effective density, and longitudinal velocity; b) altering the geometric shape of piezoceramics and using different geometric shapes (this method lacks precise control over the band gap adjustment); c) modifying the constituents of the piezocomposite, which, like the second case, results in a sudden change in the band gap parameters, hence the challenge of precise control over the band gap adjustment.

This research aims to propose a 1-3 piezocomposite of centered cubic crystal structure and investigate the effect of the volume fraction of different phases of piezoelectric rods on the band gaps while maintaining a constant ceramic filling fraction. In this analysis, Bloch-Flocke theory (Comi & Marigo, 2020) and finite element analysis were employed to study the dynamic behavior of two-dimensional piezocomposite unit cells for calculation of the band gap. A structure was also presented in this paper that allows control over the width of band gaps without altering the filling fraction, solely by changing the ηs. According to the observations, the maximum gap bandwidth was achieved in the case of η=50%.

2. Problem explanation and finite element modeling

The system under study is a 1-3 piezocomposite structure consisting of a square lattice of lattice constant "a". The unit cell comprises a pair of rods made from PZT-5H with circular cross-section and different radii, distinguishable by white and gray color, as shown in Figure 1. These PZT rods are embedded in a polymer matrix of polyethylene terephthalate.

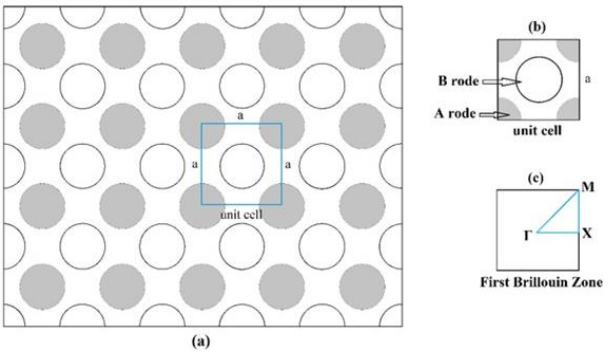

Figure 1. According to the schematic, (a) the proposed 1-3 piezocomposite network model, (b) the unite cell of the network, (c) the first Brillouin zone. Gray circles represent rode A and white circles rode B. we change the size of the gray and white circles while maintaining the filling fraction of the piezocomposite constant.

Due to the crystal periodicity and its infinite size along the x and y axes, the mechanical displacements (u_i) and electric potential (φ) follow the Bloch relation (Equations (1-2)) [15]:

$$u_i(x+ma_1,y+pa_2) = u_i(x,y,z)\exp(-jk_xma_1)\exp(-jk_ypa_2) \quad (1)$$

$$\varphi(x+ma_1,y+pa_2) = \varphi(x,y,z)\exp(-jk_xma_1)\exp(-jk_ypa_2) \quad (2)$$

where "kx" and "ky" represent the components of the Bloch wave vectors in the x and y, respectively, while m

and p are integers.

These periodical boundary conditions allow us to confine the calculations just to a single unit cell. The square unit cell of the system is also taken into account, as depicted in Figure 1-b. The cell consists of two different rode: rod A, represented by four quarter circles with the radius R_A at the corners, and rod B, a full circle with the radius R_B in the center. The polarization axis of the piezoelectric rods is considered perpendicular to the unit cell plane.

For the considered piezocomposite, the filling fraction of the piezoceramics phase, defined as the ratio of the volume of the piezocomposite rods in the unit cell to the total volume of the unit cell, is given by Equation (3).

$$(\pi(R_A^2 + R_B^2)/a^2) \tag{3}$$

Additionally, we define the volume fraction of the rod B as the ratio of the volume of rod B to the summation of the volume of the rods A and B in a unit cell, denoted by η (Equation (4)). Based on the radius of the rods, we have:

$$\eta = \frac{R_B^2}{R_A^2 + R_B^2} \tag{4}$$

The main objective of this paper is to investigate the band structures of the mentioned phononic crystal as a function of η in order to determine the optimal value of η for achieving the maximum band gap. To simplify the analysis, the filling fraction is held constant at 50% throughout this research. In other words, as the R_b increases by increasing η, R_a must decrease in such a way that the filling fraction remains constant.

Given the complex topology of this structure, a numerical method, such as the Finite Element Method (FEM), is essential to analyze the vibrational properties of the structure.

The finite element numerical method is well established for linear piezoelectric materials and has been widely used in the analysis of piezocomposites. For this reason, FEM was employed in this study to investigate the band structures of the considered composite. To this end, the unit cell is divided into a mesh of triangular elements connected by nodes as represented schematically in Figure 2.

In the absence of external forces and considering a monochromatic time dependent exp(jωt), the general piezoelectric problem is expressed by Equation (5) [14].

$$\begin{bmatrix} K_{uu} - \omega^2 M_{uu} & K_{\varphi u} \\ K_{\varphi u} & K_{uu} \end{bmatrix} \begin{pmatrix} u \\ \varphi \end{pmatrix} = \begin{pmatrix} 0 \\ 0 \end{pmatrix} \tag{5}$$

where K_{uu} and M_{uu} denote the stiffness and mass matrices of the fully elastic part of the problem, respectively. In addition, $K_{\varphi\varphi}$ and $K_{u\varphi}$ represent the pure dielectric part and piezoelectric coupling matrix, respectively. As mentioned earlier, the translational symmetry of the lattice allows us to mitigate the problem of the first Brillouin zone, as depicted in Figure 1 (b). To obtain the dispersion diagrams, the wave vector varies within the first Brillouin zone for a given propagation direction which as usual can be reduced using the symmetry properties of the system to the first irreducible Brillouin zone. For a square lattice of constant "a", the first Brillouin zone is defined by $-\pi/a<kx<\pi/a$ and $-\pi/a<ky<\pi/a$. The band structures are calculated along the M-Γ-X-M path (see Figure 1(c)). To ensure the accuracy of the results, the mesh sizes have been refined repeatedly until the angular frequency convergence is achieved.

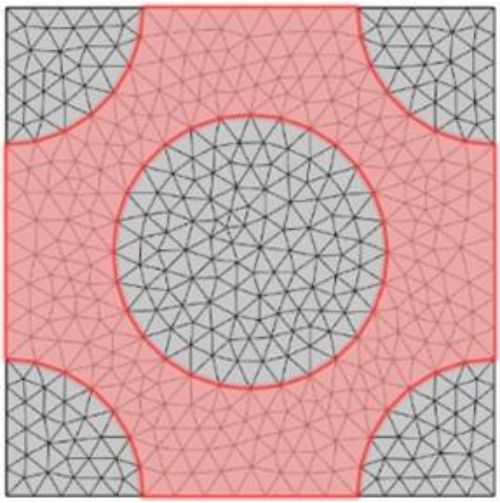

Figure 2. A view of a meshed unit cell

2. NUMERICAL SIMULATION AND DISCUSSION

This section presents and discusses the results of varying the volume fraction η and its effects on the band structure of the piezoelectric phononic crystal, introduced in the previous sections. We maintain the total filling fraction of the PZT-5H rods at a constant value of 50% while altering the η from 0 to 50%. The band structures are obtained by calculating the lowest 20 bands of the system using the finite element analysis. The material parameters used in the calculations are tabulated in Table 1, the results of which are as follow. It should be noted that since the rods within a unit cell consist of the same type of piezoceramic material, i.e., PZT-5H, we expect that the band structure for η values greater than 50% will resemble those for η<50%. In the other words, for example, the band structure of η=70% matches that of η=30% because the only difference between the unit cell in this case lies in the volumes of rods A and rods B. The bands are calculated along the path M-Γ-X-M about the irreducible Brillouin zone of the square lattice and are plotted in terms of the product of frequency and lattice

constant f × a versus the wave vector K along the first irreducible Brillouin zone, as seen in Figure 1-c. It is evident that the existing band gaps extend across the Brillouin zone, as stated by Vasseur et al. [24].

TABLE 1. Characteristics of the materials used in the calculations (Vasseur et al., 1994) (Z.-H. Qian et al., 2008)

		PZT-5H		polyethylene terephthalate
Elastic constants ($10^9 Nm^{-2}$)	C_{11}	121	Young's modulus	7×10^9
	C_{33}	117		
	C_{44}	23		
	C_{13}	84.1		
	C_{12}	79.5		
Piezoelectric constants (Cm^{-2})	e_{15}	17	Poisson's ratio	0.44
	e_{31}	-6.5		
	e_{33}	23.3		
Dielectric constants (10^{-10} F m^{-1})	ε_{13}	150	Mass Density (kg/ m^{-3})	1430
	ε_{33}	130		
Mass Density (kg/ m^{-3})	ρ	4500		

Figure 3 illustrate the band structures of the considered 1-3 piezocomposite in the limiting case η=0, which corresponds to a simple square lattice. As observed in Figure 3, there is a single complete band gap between the third and fourth bands. The gap extended in the frequency range 1100<f.a<1500 with relative bandwidth 31%.

As the η values exceeds zero, the volume of rod B starts to grow from zero as well, and due to the constant filling fraction 50%, the volume of rod A decreases.

Figure 4 (a) depicts the band structure for η=5%. In this case, the magnitude of the band gap between the third and fourth bands decrease to 209m/s. This band spans from 1105 m/s to 1314 m/s with the relative bandwidth 17%. Although this gap narrows as η increases from zero, another band gap begins to appear between the tenth and eleventh bands. This new gap falls within the frequency range of 2296 m/s to 2527 m/s with the relative band gap of 9.8%. The presence of the later gap can be attributed to the emergence of rods B in the middle of the unit cell, rather than a decrease in the volumes of rod A. To confirm this, we evaluated the band structures for very small values of η, not shown here, and observe that the later gap starts to grow immediately as η increases from zero. Given that for these small values of η, the volume of rod A does not change considerably, it is reasonable to attribute this band gap to the new scattering center produced in each unit cell. (The number in the right of each figure is the bandwidth of band gap)

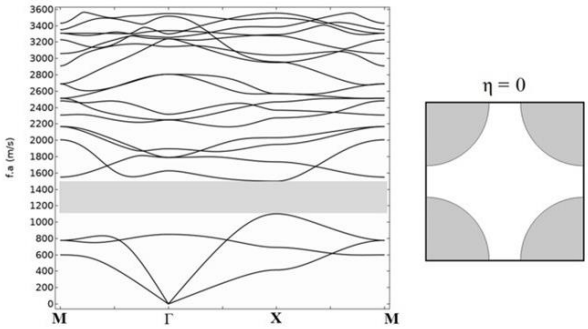

Figure 3. Dispersion diagram and elastic band structure for XY vibration modes in a typical 1-3 piezocomposite in 50% piezoceramic filling fraction, which does not have rode A circles (η=0)

TABLE 2. Specifications of materials used and different values of η

Figure	η	Polymer material	piezoceramic material	Piezoceramic filing fraction
3	0	polyethylene terephthalate (PET)	PZT-5H	50
2-(a)	5			
2-(b)	10			
2-(c)	20			
2-(d)	30			
2-(e)	40			
2-(f)	50			

Upon increasing η up to 10%, a third gap begins to emerge, as presented in Figure 4 (b). As indicated in this figure, this gap lies between the 6th and 7th bands with a lower edge at 1737m/s and relative bandwidth of 0.4%. In this case, while the lower limit of first band gap remains unchanged compared to the η =5% case, its band width decreases by 95m/s due to the descending 4th band. Contrarily, the second band gap now grows to 262m/s with the relative bandwidth of 10.9% due to the descending 10th and ascending 11th bands.

With a further increase in η up to 20%, the first band gap is closed completely as a result of the downward movement of the fourth band (in addition to the fifth and sixth bands), although the first, second, and third bands remain almost unchanged. As presented in Figure 4c, the bandwidth of the 2nd band gap shrinks symmetrically to

131 m/s, with its lower edge increasing up to 2362 m/s. On the other hand, although both the maximum of 6th band (1597m/s) and the minimum of 7th band (1791m/s) have decreased, the width of the 3rd band width increases up to 194m/s.

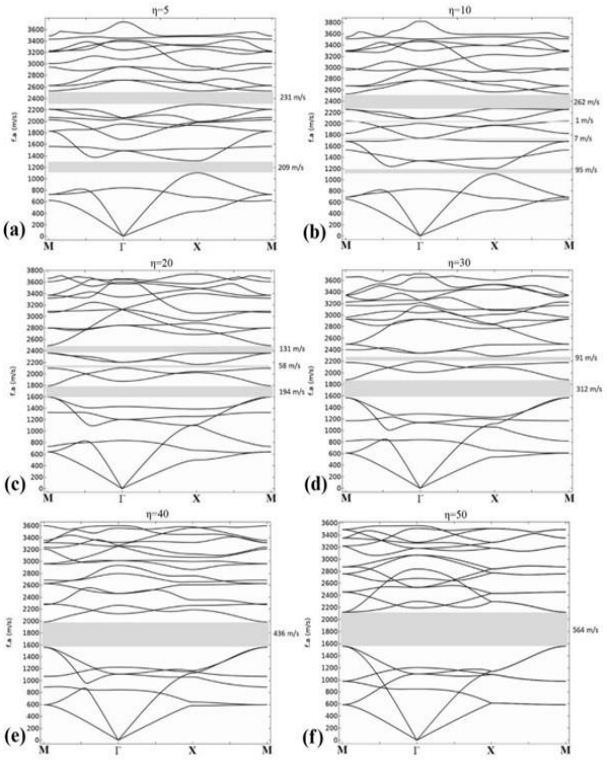

Figure 4. Dispersion diagram and elastic band structure for XY vibration modes in a typical 1-3 piezocomposite in 50% piezoceramic filling fraction

The width of the 3rd band gap grows continuously as η increases up to 50% and reaches its maximum, as depicted in Figures. 4-b, c, d, e, f. At η=50%, the 3rd gap extends in the frequency range of 2122<f.a<1558 with the band width of 564m/s and relative bandwidth of 31%. Since the 5th and 6th bands remain almost unchanged, the widening of this gap occurs as a direct result of the shift of 7th band to the higher frequencies. In addition, there is a narrower band gap just above the 7th band from η=10% to η=40%, as depicted in Figure 4-b, c, d, which is faded as η increases up to 40%. The maximum relative bandwidth of this gap is 4.3% while its minimum relative bandwidth at 2234m/s occurs at M point of Brillouin zone for η=35% (show in Figure 6). An interesting feature of the case η=50% is the dual degeneracy of each band in the X-M range. In other words, the six bands in the range of M-Γ to Γ-X converge in such a way that only three bands are observable in the X-M range. This happens mainly because for η=50%, the centered square lattice under consideration is transformed into a simple square lattice of lattice constant $a/\sqrt{2}$ whose axis rotates π/4 with respect to the axis of the centered square lattice considered so far. Figure 5 depict the Brillouin zones of this lattice as well as the original centered square. Calculation of the band structure of the simple square lattice mentioned above along with the (unconventional) directions of Figure 5 shows complete match with the η=50% case.

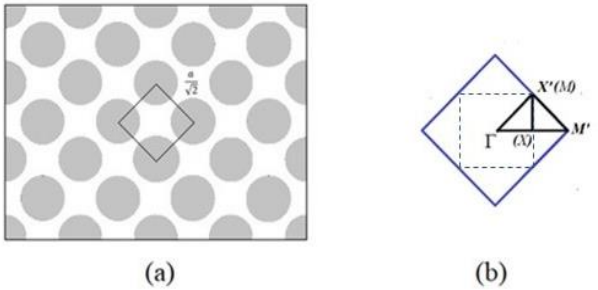

Figure 5. According to the schematic, (a) the unit cell of simple square lattice associated with = 50% (solid line), (b) The B.Z. corresponding to the simple square in addition with the B.Z. of a centered square lattice constant a of Figure 1 (The dotted lines show the Brillouin zone in Figure 1)

TABLE 2. Specifications of each band gap for different η

	1st Band gap			2nd Band gap			3rd Band gap		
η	Band end (m/s)	Band start (m/s)	Bandwidth (m/s)	Band end (m/s)	Band start (m/s)	Bandwidth (m/s)	Band end (m/s)	Band start (m/s)	Bandwidth (GHz)
0	1500	1100	400						
5	1314	1105	209	2527	2296	231			
10	1202	1107	95	2530	2268	262	1744	1737	7
15	1138	1110	28	2518	2306	212	1772	1665	107
20				2493	2362	131	1791	1597	194
25				2457	2424	33	1829	1580	249
30							1881	1569	312
35							1931	1564	367
40							1984	1548	436
45							2052	1559	493
50							2122	1558	564

In short, information of the gaps in the above-mentioned phononic crystals has been accumulated and plotted as functions of η in Figure 6. As shown in this figure, the maximum width of the first band gap, equal to 400m/s, occurs at η=0, and the gap dissolves above η=20%. In the mid-range, the second band gap dominates from η =5% up to η≈18%, with a maximum of 262m/s at η=10%. The third and the long-lasting gap start at η=10% and exists until η=50% with a maximum of 564 m/s at η=50%. The width of latter gap grows continuously with η, making it the dominant gap above η≈18%. There is also a minor gap which appears above η=10% with a

maximum not exceeding 98m/s. Finally, it should be noted that despite the nearly equal maximums of the first and second band gaps, the largest band gap, achievable by modifying the volume ratio of rode A with respect to rode B, belongs to third gap at η=50%.

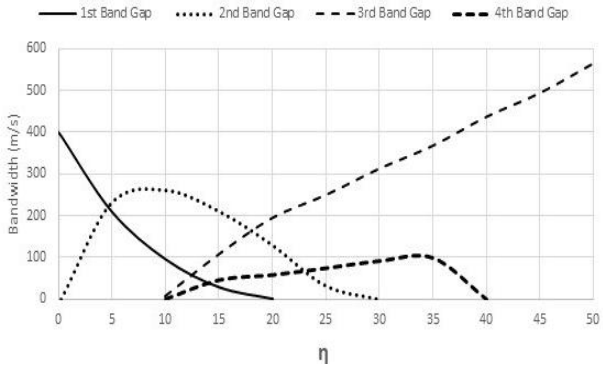

Figure 6. The width of the first five bands in terms of different values of η at the filling fraction F=50%

This property is detailed in Figure 7 which depicts the upper and lower boundaries corresponding to each gap as a function of η. As shown in this figure, the first and second band gaps lies in the frequency ranges of 1500 m/s-1100 m/s and 2268 m/s-2530 m/s, respectively, with the third gap in between ranging from 1558 m/s to 2122 m/s. Of note, no gap exists below the lower frequency limit of first gap and above the higher frequency limit of the second band gap (although it has been tested but not presented here by considering 50 bands in our calculations).

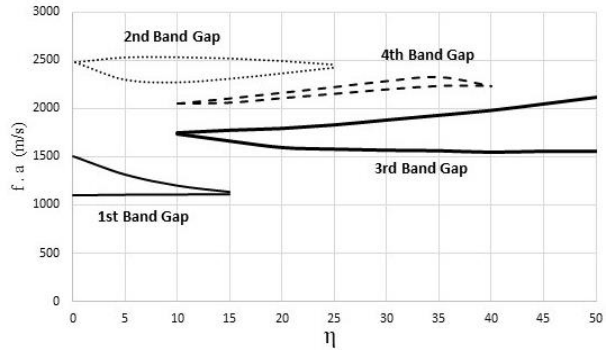

Figure 7. The open points, close points and width of the band gaps at the filling fraction F=50% versus η

We calculated the density of states in the entire Brillouin zone, which is shown as an example of the results obtained for a filling fraction=50% and eta = 50% in Figure 8. According to the obtained results, this gap is spread throughout the Brillouin zone. The presence and magnitude of this gap in the elastic band structure and density of state clearly show that this band gap extends throughout the Brillouin zone.

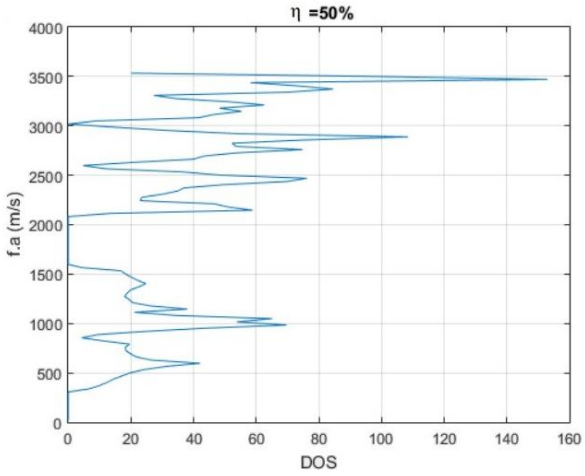

Figure 8. The density of states at the filling fraction F=50% versus η=50%

The bandwidth, lower and upper limits, and opening and closing points of each band gap in different η values are easily detectable in Figure 7. In the first and third band gaps, the lower limit of the band gap is almost constant, and their changes are mainly caused by changes in their upper limit. According to Figure 4, the first, second, and third bands remain stable and unchanged and with the movement of the fourth, fifth, and sixth modes, the first band gap closes. After the first band gap closes, these modes remain almost constant and unchanged, thus playing a role as the lower limit of the third band gap. With the stability of these modes, the main changes in the bandwidth of the third band result from the upward movement of the higher bands. In other words, in case the bandwidth of the third band gap increases, the first to sixth modes remain constant and unchanged, and the main change of this band gap results from the upward movement of the seventh, eighth, ninth, and tenth bands. In general, it can be concluded that addition of the rode A creates new boundary conditions and excites lateral modes, and these new boundary conditions lead to changes in the band gaps.

As shown in Figure 4, by changing the η while maintaining the filling fraction of the piezoceramic rods, the dispersion diagram of the piezocomposite changes, showing that the band gaps are highly sensitive to these changes, and this parameter can be adjusted to obtain a larger relative bandwidth in the desired frequency range.

Upon comparing Figure 3 (η=0) with other figures, it can be concluded that this method allows us to create band gaps in different frequency ranges and different widths. In addition, in the η=50 (Figure 4 (f)), the bandwidth of the band gap is 1.43 times that of the mode without rode B (η =0) (Figure 3). In some values of η, we have two or three bands at the same time at different frequency ranges. According to the diagrams, the changes in the bands are attributed to the displacement of higher modes and their movement towards higher or

lower frequencies. In this respect, it can be concluded that the non-uniform volume distribution of piezoceramic rods cause these changes.

With the increase of η, phase b elements appear from zero while their effect gradually increases. These elements are located between the elements of phase A, reducing the distance between then, and as a result. As a result, it is expected that the forbidden gap at low frequencies will gradually disappear and shift to higher frequencies. As observed in Figure 4, this effect occurs by transferring the frequency modes to the forbidden gap. While the energy of the lowest three frequency bands remains almost constant, the frequency of its upper edge gradually decreases.

The first energy gap is caused by the destructive combination of waves moving in the x or y direction and being partially reflected from the plates containing the phase A elements. Reducing the volume of phase A elements and increasing the effect of phase B elements on these reflections upon increasing η reduces the size of this gap until finally it disappears for η=15 by decreasing the energy of the fourth frequency band.

On the other hand, the second frequency gap appears immediately with an increase in η from zero. Due to the high frequency of this gap, its creation can be attributed to the destructive combination of waves that move perpendicular to the planes of phases a and b (along the x or y axes) and are partially reflected from these phases. Initially, the width of this gap increases with an increase in η bit it ultimately closes by reducing the frequency of its upper edge and increasing the energy of its lower edge at η=0.25.

The third energy gap, which is the main focus in this research, starts to appear from η=10. This gap is created by the destructive superposition of waves that move along the bisector of the x and y axes and being partially reflected from the phase elements A and B. Increasing the volume of phase B and the simultaneously decreasing the volume of phase A with an increase in η bring the volume of these two elements closer together. As a result, the width of the gap increases continuously with the increase of η until at η=50, where the volume of the two elements becomes equal, the gap reaches its maximum value. At η=50, the final grid is a simple square grid, rotated by 45 degrees relative to the initial grid at η=0, and the distance between its elements is a/sqrt (2). Hence, the width of the gap in this case is sqrt (2) times that of η=0.

We calculated the entire inverted space and observed that this gap has extended throughout entire inverted space.

In previous research, such as the study by Zhang Hua et al. [15], changes in the filling fraction of piezoceramic were typically used to alter the bandgap, resulting in changes in the functional characteristics of the piezoceramic, such as effective electromechanical coupling coefficient, characteristic impedance, longitudinal velocity, and density. However, in this case, without changing the piezoceramic filling fraction, the bandwidth and location of the band gaps can be controlled without changing the piezoceramic filling fraction, allowing for the desired bandwidth and location based on practical needs.

3. CONCLUSION

In the current research, the phononic band structures of a two-dimensional body center 1-3 piezocomposite consisting of PZT-5H rod and polyethylene terephthalate polymer matrix were theoretically investigated. The volume fraction of the PZT rods was assumed to be constant as 50% to examine the band structure of the system as a function of the ratio η, representing the volume fraction of the PZT rod at the center of a unit cell relative to the total volume of the PZT rods in the unit cell. The results revealed that in the whole range of variation of η, there was at least one complete band gap in the band structure of the considered structure while detecting no gaps below f.a=110 m/s and above f.a=2530 m/s. Moreover, the band structure contained three main band gaps (in addition to two minor ones) that reached their maximum values at η=0% (first band gap), η=20% (second band gap), and η=50% (third band gap), the latter is the largest band gap (equal to 564m/s) of the considered system.

ACKNOWLEDGEMENTS

The authors would like to acknowledge Payame Noor University and Malek Ashtar University for all supports throughout this work.

REFERENCES

1. Amanat, B. (2022). "Improvement of the Effective Parameters of 1-3 Piezocomposite Using Multi-Layer Polymer and PMN-PT Relaxor Single Crystal." ***Advanced Ceramics Progress***, 8(2), 61–72. https://doi.org/10.30501/acp.2022.355196.1099
2. Behera, A. (2022). "***Piezoelectric Materials. In A. Behera (Ed.), Advanced Materials: An Introduction to Modern Materials Science***", (pp. 43–76). Springer International Publishing. https://doi.org/10.1007/978-3-030-80359-9_2
3. Comi, C., & Marigo, J.-J. (2020). "Homogenization Approach and Bloch-Floquet Theory for Band-Gap Prediction in 2D Locally Resonant Metamaterials." ***Journal of Elasticity***, 139. https://doi.org/ 10.1007/s10659-019-09743-x
4. Halkjaer, S., Sigmund, O., & Jensen, J. (2005). "Inverse design of phononic crystals by topology optimization." ***Zeitschrift Fur Kristallographie - Z KRISTALLOGR***, 220, 895–905. https://doi.org/ 10.1524/zkri.2005.220.9-10.895
5. Halkjær, S., Sigmund, O., & Jensen, J. (2006). "Maximizing band gaps in plate structures." ***Structural and Multidisciplinary Optimization***, 32, 263–275. https://doi.org/10.1007/s00158-006-0037-7
6. Hou, Z., Wu, F., & Liu, Y. (2004). "Phononic crystals containing piezoelectric material.", ***Solid State Communications***, 130(11), 745–749. https://doi.org/10.1016/j.ssc.2004.03.052
7. Lv, J., Xie, X., Zhu, X., Li, Z., Han, Z., Cui, Y., Zhang, B., & Jian, X. (2022). "Cold ablated high frequency PMN-PT/Epoxy 1-3 composite transducer.", ***Applied Acoustics***, 188, 108540. https://doi.org/10.1016/j.apacoust.2021.108540

8. Miranda, E. J. P., & Dos Santos, J. M. C. (2022). "Wave attenuation in 1-3 phononic structures with lead-free piezoelectric ceramic inclusions.", ***Physica B: Condensed Matter***, 631, 413642. https://doi.org/10.1016/j.physb.2021.413642
9. Qian, Z., Jin, F., Wang, Z., & Kishimoto, K. (2004). "Dispersion relations for SH-wave propagation in periodic piezoelectric composite layered structures.", ***International Journal of Engineering Science***, 42(7), 673–689. https://doi.org/10.1016/j.ijengsci.2003.09.010
10. Qian, Z.-H., Jin, F., Li, F.-M., & Kishimoto, K. (2008). "Complete band gaps in two-dimensional piezoelectric phononic crystals with {1–3} connectivity family.", ***International Journal of Solids and Structures***, 45(17), 4748–4755. https://doi.org/10.1016/j.ijsolstr.2008.04.012
11. Rupp, C., Evgrafov, A., Maute, K., & Dunn, M. (2007). "Design of phononic materials/structures for surface wave devices using topology optimization.", ***Structural and Multidisciplinary Optimization***, 34, 111–121. https://doi.org/10.1007/s00158-006-0076-0
12. Sigmund, O., & Jensen, J. (2003). "Systematic design of phononic band-gap materials and structures by topology optimization.", ***Philosophical Transactions. Series A, Mathematical, Physical, and Engineering Sciences***, 361, 1001–1019. https://doi.org/ 10.1098/rsta.2003.1177
13. Thompson, J. M. T., & Sigmund, O. (2000). "Topology optimization: A tool for the tailoring of structures and materials.", ***Philosophical Transactions of the Royal Society of London. Series A: Mathematical, Physical and Engineering Sciences***, 358(1765), 211–227. https://doi.org/10.1098/rsta.2000.0528
14. Tize Mha, P., Maréchal, P., Ntamack, G. E., and Charif d'Ouazzane, S. (2021). "Homogenized electromechanical coefficients and effective parameters of 1–3 piezocomposites for ultrasound imaging transducers.", ***Physics Letters A***, 408, 127492. https://doi.org/ 10.1016/j.physleta.2021.127492
15. Vashishth, A. K., & Gupta, V. (2009). "Wave propagation in transversely isotropic porous piezoelectric materials.", ***International Journal of Solids and Structures***, 46(20), 3620–3632. https://doi.org/10.1016/j.ijsolstr.2009.06.011
16. Vasseur, J. O., Djafari-Rouhani, B., Dobrzynski, L., Kushwaha, M. S., & Halevi, P. (1994). "Complete acoustic band gaps in periodic fibre reinforced composite materials: The carbon/epoxy composite and some metallic systems.", ***Journal of Physics Condensed Matter***, 6, 8759–8770. https://doi.org/10.1088/0953-8984/6/42/008
17. Vatanabe, S. L., Paulino, G. H., & Silva, E. C. N. (2014). "Maximizing phononic band gaps in piezocomposite materials by means of topology optimization.", ***The Journal of the Acoustical Society of America***, 136(2), 494. https://doi.org/10.1121/1.4887456
18. Vatanabe, S. L., & Silva, E. C. N. (2011). "Design of phononic band gaps in functionally graded piezocomposite materials by using topology optimization.", ***Behavior and Mechanics of Multifunctional Materials and Composites*** 2011, 7978, 268–277. https://doi.org/10.1117/ 12.878851
19. Vu Quoc, T., Do Ba, D., Tran Thi Thuy, D., Nguyen Ngoc, L., Nguyen Thuy, C., Vu Thi, H., Khanh, L. D., Doan Thi Yen, O., Thai, H., Long, V. C., Talu, S., & Nguyen Trong, D. (2021). "DFT study on some polythiophenes containing benzo[d]thiazole and benzo[d]oxazole: Structure and band gap.", ***Designed Monomers and Polymers***, 24(1), 274–284. https://doi.org/10.1080/15685551.2021.1971376
20. Wang, H., Li, Y., Hui, H., & Rong, T. (2022). "Analysis of electromechanical characteristics of the 1-3-2 piezoelectric composite and 1-3-2 modified structural material.", ***Ceramics International***, 48(15), 22364–22375. https://doi.org/10.1016/j.ceramint.2022.04.238
21. Wang, Y.-S. (2008). "Calculation of band structures for surface waves in two-dimensional phononic crystals with a wavelet-based method.", ***Phys. Rev. B***, 78. https://doi.org/10.1103/PhysRevB.78.094306
22. Wang, Y.-Z., Li, F.-M., Huang, W.-H., & Wang, Y.-S. (2007). "Effects of inclusion shapes on the band gaps in two-dimensional piezoelectric phononic crystals.", ***Journal of Physics: Condensed Matter***, 19, 496204. https://doi.org/10.1088/0953-8984/19/49/496204
23. Wang, Y.-Z., Li, F.-M., Kishimoto, K., Wang, Y.-S., & Huang, W.-H. (2009). "Wave band gaps in three-dimensional periodic piezoelectric structures.", ***Mechanics Research Communications***, 36(4), 461–468. https://doi.org/10.1016/j.mechrescom.2009.01.003
24. Wu, M.-L., Wu, L.-Y., Yang, W.-P., & Chen, L.-W. (2009). "Elastic wave band gaps of one-dimensional phononic crystals with functionally graded materials.", ***Smart Materials and Structures***, 18, 115013. https://doi.org/10.1088/0964-1726/18/11/115013
25. Zhou, C., Zhang, J., Liu, D., & Zhang, Z. (2021). "Novel 1–3 (K,Na)NbO_3-based ceramic/epoxy composites with large thickness-mode electromechanical coupling coefficient and good temperature stability.", ***Ceramics International***, 47(4), 4643–4647. https://doi.org/ 10.1016/j.ceramint.2020.10.031